07AC-86

Transient Characteristics of a Hydraulically Interconnected Suspension System

J. M. Jeyakumaran, W. A. Smith and N. Zhang

Mechatronics and Intelligent Systems, University of Technology, Sydney, Australia

ABSTRACT

This paper describes vehicle dynamic models that capture the large amplitude transient characteristics of a passive Hydraulically Interconnected Suspension (HIS) system. Accurate mathematical models are developed to represent pressure-flow characteristics, fluid properties, damper valves, accumulators and nonlinear coupling between mechanical and fluid systems. The vehicle is modeled as a lumped mass system with half- and full-car configurations. The transient performance is demonstrated by numerical integration of the second-order nonlinear differential equations. The stiffness and damping characteristics corresponding to vehicle bounce, roll and pitch motions are extracted from the transient simulation. Simulation results clearly demonstrate the superiority of the HIS system during vehicle handling and stability by providing additional roll stiffness and reduced articulation stiffness.

INTRODUCTION

The design of vehicle suspension systems involves a compromise between ride comfort and vehicle handling [1-3]. A softer suspension yields good ride performance with the expense of poor stability and directional control. Alternatively, a stiffer suspension enhances handling and minimizes the occurrence of vehicle rollover, yet it provides poor ride comfort. In recent decades, several suspension systems varying from passive to semi-active to fully active have been proposed to break the compromise between ride comfort and handling [4-10]. With the rapid development of sensing technologies, the recent trends are largely towards active, semi-active and slow-active suspension systems, and the superiority of these systems has been established in luxury passenger vehicles [11-13]. In principle, active and semi-active suspension systems have the greatest capability to achieve optimum performance, however, the inherent drawbacks are the weight, cost, uncertain reliability, increased power consumption and complexity. Because of challenges associated with active controls with minimum hardware, the passive suspensions that enhance vehicle handling and stability are still of great interest for vehicle manufacturers.

Suspension researchers have paid attention to more effective passive systems that interconnect suspension actions between left and right, front and rear wheel-stations to provide optimal stiffness in bounce, pitch and roll motions. There are several interconnected vehicle suspensions acquainted in the automotive market [14, 15]. The anti-roll bars are the simplest and most commonly used interconnected system. Early examples of interconnections also include Citroen interconnected coil springs and Moulton's hydro-elastic suspensions. Published results show that the interconnected systems are very effective in reducing vehicle bounce, pitch or roll, as compared to independent suspension units. However, only limited systematic investigations have been attempted on the dynamics of vehicles fitted with interconnected systems.

In mid 1990s, Rakheja *et al*. [16] and Liu *et al.* [17, 18] investigated a Hydraulically Interconnected Suspension (HIS) system to predict vehicle ride and handling performance. They developed fluid dynamics models to include the effects of fluid compressibility, valve characteristics and adiabatic process of confined gas, and integrated them in a four-degree-of-freedom vehicle model. They demonstrated that enhanced roll stiffness and damping characteristics of the HIS provide improved roll stability and ride performance characteristics. However, complex fluid properties such as the nonlinear mechanical and fluid couplings, fluid inertia and wave propagation effects are not included in their mathematical models. Recently, more novel HIS systems have been reported [19-22] and the superiority of these systems was demonstrated experimentally using the US National Highway Traffic Safety Administration's (NHTSA) *Fishhook Maneuver* [23, 24]. Vehicle testing is used as the main tool for improving the HIS dynamic characteristics, however, this requires much effort and time during the product development process.

Recently, Nong *et al.* [25] has developed an efficient half-car model for the vibration analysis of a vehicle fitted with a HIS system. The most obvious limitation of

that study was its linearity, i.e., the nonlinearities associated with the cylinder volume coupling, the accumulator *air-spring* effect, and damper valve characteristics were not included in the model formulation. In linear models, the parameters of the hydraulic oil are held constant, and therefore the pressure- and temperature-dependence of the fluid bulk modulus, viscosity and density are neglected. The coupling between mechanical and fluid systems, damper valve characteristics and variations in fluid properties are significant nonlinearities of the HIS and ride evaluation requires accurate modelling of these nonlinearities [26, 27]. In addition, the hydraulic elements feature high fluid velocities, pressures and accelerations during fast transients, and therefore the analysis method requires numerical integration.

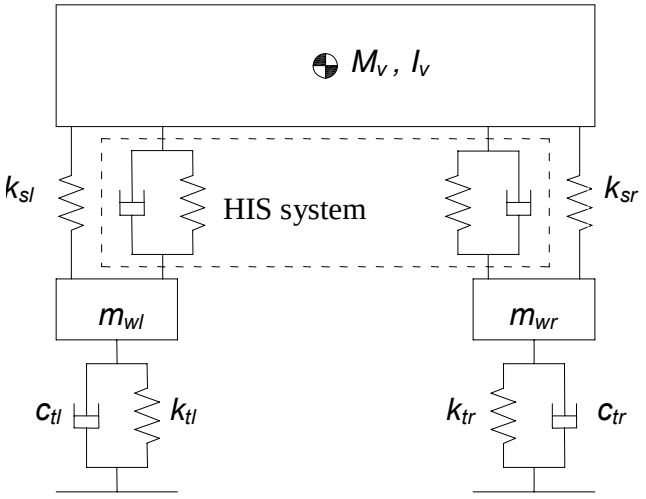

Figure 1: Schematic diagram of the HIS system in roll-plane

In this paper, a mathematical model that captures the large amplitude transient characteristics of a HIS is presented. The transient responses of the vehicle, measured by its roll, bounce and pitch motions are investigated numerically using specified impulsive forces and moments. Simulation of the fluid exchanges/dynamics is carried out from the set of second-order differential equations describing the HIS system. In the next section, the roll-plane models of the mechanical and hydraulic system are presented. Similarly, the full vehicle is modelled as a lumped mass system with seven-degrees-of-freedom, i.e., the pitch, roll, and bounce motions of the vehicle and vertical movements of the four wheel-stations. Because of the commercial sensitivity of the full-car HIS system, a detailed derivation of the seven-degrees-of-freedom model is not presented. The simulation results are presented for specific impulsive loads applied at the centre of gravity of the sprung mass. The effective stiffness and damping coefficients corresponding to vehicle roll, bounce and pitch motions are extracted from the transient simulation.

MODEL FORMULATION

MECHANICAL SYSTEM MODEL

The schematic diagram of a half-car model fitted with a HIS system in roll-plane is shown in Figure 1. The conventional shock absorbers and anti-roll bar assemblies between sprung vehicle body and unsprung wheel-stations are replaced with a HIS system. The vehicle is represented with a lumped four-degree-of-freedom system to include vehicle roll and bounce motions and vertical movements of two wheel-stations. The lateral and yaw motions of the vehicle are not included in the formulation. The stiffness and damping of the tires linked to the wheel-stations are included. The cylinder component is assumed as rigid in the horizontal directions. Figure 2 shows the Free Body Diagram (FBD) of the half-car model.

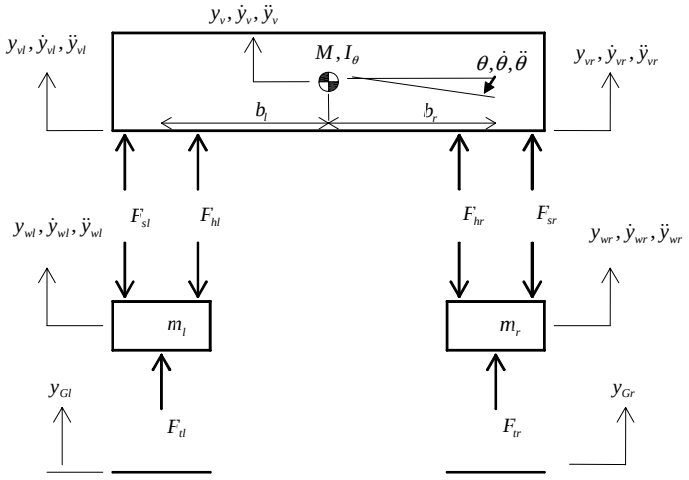

Figure 2: Free body diagram of the half-car model

The equations of motion of the half-car mass and two wheel masses are derived from Newton's second law of motion. From the FBD of the left and right wheels, we have:

$$m_l\ddot{y}_{wl} = k_{tl}\left(y_{Gl} - y_{wl}\right) + c_{tl}\left(\dot{y}_{Gl} - \dot{y}_{wl}\right) - k_{sl}\left(y_{wl} - y_{vl}\right) - c_{sl}\left(\dot{y}_{wl} - \dot{y}_{vl}\right) - F_{kl} \quad (1)$$

$$m_r\ddot{y}_{wr} = k_{tr}\left(y_{Gr} - y_{wr}\right) + c_{tr}\left(\dot{y}_{Gr} - \dot{y}_{wr}\right) - k_{sr}\left(y_{wr} - y_{vr}\right) - c_{sr}\left(\dot{y}_{wr} - \dot{y}_{vr}\right) - F_{kr} \quad (2)$$

From the FBD of the vehicle body shown in Figure 2:

$$M\ddot{y}_v = k_{sl}\left(y_{wl} - y_{vl}\right) + c_{sl}\left(\dot{y}_{wl} - \dot{y}_{vl}\right) + k_{sr}\left(y_{wr} - y_{vr}\right) + c_{sr}\left(\dot{y}_{wr} - \dot{y}_{vr}\right) + F_{kl} + F_{kr} \quad (3)$$

$$I_\theta \ddot{\theta} = -b_l k_{sl}\left(y_{wl} - y_{vl}\right) - b_l c_{sl}\left(\dot{y}_{wl} - \dot{y}_{vl}\right) + b_r k_{sr}\left(y_{wr} - y_{vr}\right) + b_r c_{sr}\left(\dot{y}_{wr} - \dot{y}_{vr}\right) - b_l F_{kl} + b_r F_{kr} \quad (4)$$

The equation of motion for the integrated model is:

$$[\mathbf{M}]\{\ddot{\mathbf{Y}}\} + [\mathbf{C}]\{\dot{\mathbf{Y}}\} + [\mathbf{K}]\{\mathbf{Y}\} = \{\mathbf{F}\} \quad (5)$$

where $\{\mathbf{Y}\}, \{\dot{\mathbf{Y}}\}$ and $\{\ddot{\mathbf{Y}}\}$ are the displacement, velocity, acceleration vectors and are given by

$$\{\mathbf{Y}\}, \{\dot{\mathbf{Y}}\}, \{\ddot{\mathbf{Y}}\} = \begin{Bmatrix} y_{wl} \\ y_{wr} \\ y_v \\ \theta \end{Bmatrix}, \begin{Bmatrix} \dot{y}_{wl} \\ \dot{y}_{wr} \\ \dot{y}_v \\ \dot{\theta} \end{Bmatrix}, \begin{Bmatrix} \ddot{y}_{wl} \\ \ddot{y}_{wr} \\ \ddot{y}_v \\ \ddot{\theta} \end{Bmatrix}$$

In Eq. (5), mass, damping and stiffness matrices, [**M**], [**C**] and [**K**] are 4x4 matrices with constant coefficients and are given by

$$[\mathbf{M}] = \begin{bmatrix} m_l & 0 & 0 & 0 \\ 0 & m_r & 0 & 0 \\ 0 & 0 & M & 0 \\ 0 & 0 & 0 & I_\theta \end{bmatrix}$$

$$[\mathbf{C}] = \begin{bmatrix} c_{tl} + c_{sl} & 0 & -c_{sl} & b_l c_{sl} \\ 0 & c_{tr} + c_{sr} & -c_{sr} & -b_r c_{sr} \\ -c_{sl} & -c_{sr} & c_{sl} + c_{sr} & -b_l c_{sl} + b_r c_{sr} \\ b_l c_{sl} & -b_r c_{sr} & -b_l c_{sl} + b_r c_{sr} & b_l^2 c_{sl} + b_r^2 c_{sr} \end{bmatrix}$$

$$[\mathbf{K}] = \begin{bmatrix} k_{tl} + k_{sl} & 0 & -k_{sl} & b_l k_{sl} \\ 0 & k_{tr} + k_{sr} & -k_{sr} & -b_r k_{sr} \\ -k_{sl} & -k_{sr} & k_{sl} + k_{sr} & -b_l k_{sl} + b_r k_{sr} \\ b_l k_{sl} & -b_r k_{sr} & -b_l k_{sl} + b_r k_{sr} & b_l^2 k_{sl} + b_r^2 k_{sr} \end{bmatrix}$$

The force vector, {**F**}, is dependent on the hydraulic system couplings and specified vertical rise/fall of the road profile to the individual wheels. In particular,

$$\{\mathbf{F}\} = \{\mathbf{F_G}\} + \{\mathbf{F_K}\} = \begin{Bmatrix} c_{tl}\dot{y}_{Gl} + k_{tl} y_{Gl} \\ c_{tr}\dot{y}_{Gr} + k_{tr} y_{Gr} \\ 0 \\ 0 \end{Bmatrix} + \begin{Bmatrix} -F_{kl} \\ -F_{kr} \\ F_{kl} + F_{kr} \\ -b_l F_{kl} + b_r F_{kr} \end{Bmatrix} \quad (6)$$

It is assumed that the mechanical suspension is linear and tire consists of a linear spring-damper combination.

HYDRAULIC SYSTEM MODEL

The hydraulic schematic diagram of the half-car HIS system is shown in Figure 3. This is a completely interconnected system and it replaces the conventional shock absorbers and anti-roll bar assemblies with interconnected hydraulic cylinders, accumulators, damper valves and fluid pipelines. The cylinders are kinetically linked to the two wheel-stations and the chassis. The hydraulic elements are arranged such that vehicle bounce, pitch and roll motions operate with fluid flow through selected accumulators and dampers. The velocities and the forces applied to the pistons from the wheel-stations cause changes in the pressures and flow rates in the fluid circuits. The vertical velocities and the forces applied to the pistons at the four wheel-stations are defined as the physical states (inputs) and the pressures and flow rates in the cylinders as the system states (outputs). The interconnections between these system physical states are determined by applying the kinetic principles to the motions of pistons and cylinders, and the motion of the fluids.

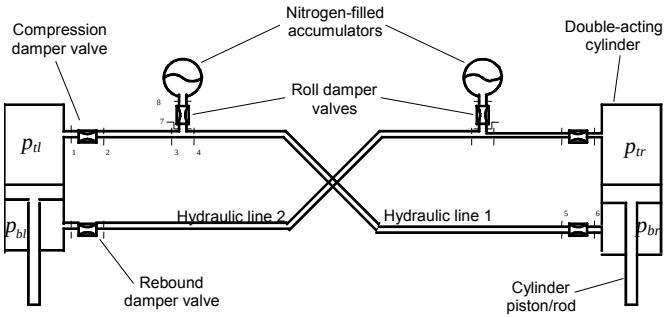

Figure 3: Hydraulic Schematic diagram of the half-car HIS system

The hydraulic system shown in Figure 3 is complex and each hydraulic element requires careful mathematical treatment to represent the dynamic characteristics of the overall system. Accurate models are developed to represent the dynamics of pistons, damper valves and upper and lower cylinder chambers. The oil aeration is a significant nonlinearity in models of hydraulic circuits and it is an important parameter for the dynamic analysis. The fluid bulk modulus is modified to account for the air in the oil, and flexibility of hoses and pipelines. The differential equations that describe the pressure changes in terms of various system flow quantities can be written in the following generalized form

$$\dot{p} = \frac{\beta(p)}{V} \sum Q \quad (7)$$

where ΣQ represents the net flow to the fluid volume. The value $\beta(p)$ is a linear function of pressure. The flow rates passing through the bleed holes, damper valves, frestrictions in fluid lines and accumulators are described by standard turbulent orifice flow equations, i.e.,

$$Q = c_d A_0 \sqrt{(p_1 - p_2)} \quad (8)$$

The pressure drop and flow resistance in the annular flows are dominated by the viscosity effect rather than the orifice flow, thus the pressure drop due to viscosity effects is incorporated in fluid lines connecting hydraulic elements.

Damper Valve Characteristics

The damper valves play an important role in the HIS system performance. The relationship between flow rate and pressure drop of the dampers is highly nonlinear, and simulation of such element requires modelling the interactions between fluid flow and cylinder-piston stroke [27, 28]. The damper valve provides high damping associated with bleed flows corresponding to lower strut velocities and low damping associated with flows through valves corresponding to high velocity. The valves are designed to provide greater resistance in one direction of the piston moment than the other. A typical valve characteristics is defined by the relationship between the volumetric flow rate and pressure difference as shown in Figure 4. The valve characteristics are divided into three regions: a valve closed region, transient region and valve open region. During the steady state conditions, the valve is fully closed and flow is allowed through small bleed holes. During fast transients, the valve is fully open and the flow characteristics are determined from the valve dynamics and stiffness properties of the valve springs. In the transient region, the valve is partially open to provide smooth transition in flow characteristics and damping force.

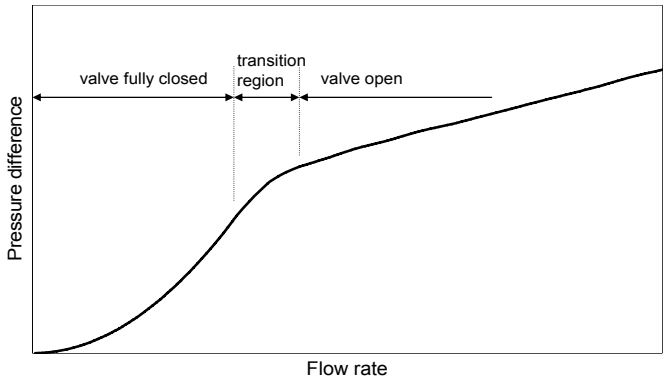

Figure 4: A typical damper valve characteristics of the HIS system

The equation of motion of the damper valves and cylinder-pistons is primarily dictated by pressure forces, spring forces, damping forces and flow forces and can be written in the following generalized form:

$$F_p + F_s + F_d + F_f = m_s \ddot{x}_s \tag{9}$$

In the half-car configuration, the equations of motion of four cylinder-damper valves, two accumulator valves and cylinder-pistons are derived and coupled with the four-degree-of-freedom mechanical system model.

Pipelines

The vehicle layout and packaging constraints of the HIS system requires relatively long flexible pipelines. A lumped parameter model is developed by dividing the fluid pipelines into several elements. The fluid pipe of constant diameter is handled as one element. Figure 5 shows a pipeline element *i* with a constant diameter. The mean pressure and mean flow in each element is assumed as an arithmetic mean of the pressure and flow rate at both ends of the pipe. The fluid flow is assumed as one-dimensional compressible flow to accommodate the water hammer phenomenon.

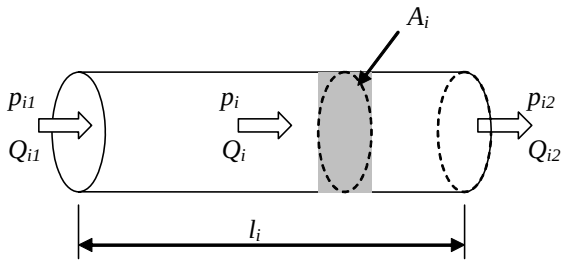

Figure 5: A model of the pipeline element *i* with a constant diameter

Assuming the pressure losses due to viscosity are proportional to the mean flow rate, and the magnitude of losses is the same as the inertia and pressure forces, the momentum equation can be written as

$$\frac{\rho l_i}{A_i}\dot{Q}_i = (p_{i1} - p_{i2}) - k_i\, l_i\, Q_i \tag{10}$$

where the viscous loss factor $k_i = 8\pi\upsilon\rho / A_i^2$. The continuity equation for the pipeline is written in terms of the mean pressure and flow difference between the ends of the pipe element as

$$\dot{p}_i = \frac{\beta(p)}{V_i}(Q_{i1} - Q_{i2}) \tag{11}$$

where *β(p)* is defined in Eq. (7). The mean pressure and mean flow rate of the pipe element is given as the arithmetic mean at both ends of the element, i.e.,

$$p_i = \frac{1}{2}(p_{i1} + p_{i2})\ ; \quad Q_i = \frac{1}{2}(Q_{i1} + Q_{i2}) \tag{12a, b}$$

In general, the pipe ends are connected by a junction point. If the net flows to the junction are denoted by $Q_{i1,\ in}$ and $Q_{i2,\ out}$ then taking time derivative of Eq. (12a) and applying continuity equation for the junctions, we have

$$\frac{2\beta(p)}{V_i}(Q_{i1} - Q_{i2}) = \frac{\beta(p_{i1})}{V_{i1}}(Q_{i1,\ in} - Q_{i1}) + \frac{\beta(p_{i2})}{V_{i2}}(Q_{i2} - Q_{i2,\ out}) \tag{13}$$

Eqs. (10), (12b) and (13) describes the fluid flow with unknown flow rates Q_i , Q_{i1} and Q_{i2}. It is noted that the equation of motion of the next pipeline is function of Q_{i1} and Q_{i2}, and therefore a system of coupled equations is formulated for the pipeline.

Accumulator Model

As shown in Figure 3, the HIS system features gas-pressurized hydraulic accumulators to reduce shock pressure loading due to system inputs. The accumulator consists of a pressure housing divided into two chambers by an elastometric diaphragm. One chamber is filled with gas and the other chamber filled with hydraulic fluid. The compressibility of the oil in the accumulator is neglected, as the oil stiffness is much greater than that of the nitrogen contained in the bladder. A drop in the system pressure is accompanied by flow from the accumulator and therefore the accumulator needs to be sufficiently large to meet the peak flow demands without appreciable drop in the system pressure. Accumulators also supply high transient flow when required for short periods and they determine the system pressure. The accumulator is modeled by assuming an adiabatic process [29].

$$pV^{\gamma} = p_o V_o^{\gamma} = \text{const.} \tag{14}$$

The adiabatic gas law is used to model the accumulator pressure as a function of gas volume at a precharged pressure. Taking partial time derivative of Eq. (14) noting that the flow into the accumulator *Q*, is given by $Q = -\partial V / \partial t$, the pressure gradient of the accumulator can be written as a nonlinear function of pressure *p*

$$\dot{p} = \frac{\gamma Q\, p}{V_o}\left(\frac{p}{p_o}\right)^{1/\gamma} \tag{15}$$

The numerical integration of Eq. (15) is carried out to determine accumulator pressure.

Model simulation

The transient responses of the vehicle, measured by its motion in roll, bounce and pitch is investigated numerically using specified inputs under typical operating conditions. The simulation is performed with Advanced Continuous Simulation Language (ACSL), an AcslXtreme product distributed by AEgis technologies. The system is solved by Runge-Kutta-Fehlberg fourth order integration with variable time steps. In general, the nonlinear system of equations of the hydraulic system is very stiff and requires extensive numerical computations. Time histories of displacements, velocities and accelerations are recorded for half- and full-car configurations. In addition, hydraulic system parameters such as cylinder chamber and accumulator pressures, pressure losses in the pipe lines, junctions and damper valves, flow demands to cylinder chamber, gas volume, etc., are recorded at each communication interval.

RESULTS AND DISCUSSION

In order to demonstrate the transient characteristics of the HIS system, the developed half- and full-car models are simulated with various impulsive forces. In particular, large amplitude roll, bounce and pitch impulse inputs of various magnitudes with duration of 0.01 sec are specified at the centre of gravity of the sprung mass (vehicle body). The time history of selected vertical displacements and typical hydraulic system pressures are presented. The effective stiffness and damping coefficients during roll, bounce and pitch motions are calculated from the vehicle displacements. The validity of dynamic properties of the half-car model is assessed against those of the full-car model. The mechanical and hydraulic system parameters used for the half-car simulation are presented in Tables 1 and 2. Because of the commercial sensitivity the hydraulic schematic of the full-car HIS and system parameters of certain hydraulic elements such as cylinders, pipelines and damper valves are not provided.

Table 1: Mechanical system parameters

Symbol	Value	Units
M	700	kg
m_j	50	kg
I_θ	250	kg/m^2
b_j	0.75	m
k_{sj}	20	kN/m
k_{tj}	200	kN/m
c_{tj}	3000	N.s/m
c_{kj}	100	N.s/m

Table 2: Hydraulic system parameters

Symbol	Value	Units
ρ	870	kg/m^3
μ	0.05	N.s/m^2
β	1400	MPa
d	7.07	mm
t_p	2.0	mm
E	210	GPa
V_p	200	ml
P_p	0.5	MPa
γ	1.45	-

Figures 6 and 7 show the simulation results of the half-car model when an impulsive roll moment of 50 kNm is

applied at the centre of gravity of the sprung mass. This roll moment simulates the dynamic characteristics of the HIS system during high amplitude roll motion at high roll rates. In particular, the impulsive moment simulates an initial maximum role rate of 105 deg/sec. This roll rate is nearly twice as large as the maximum value of about 52 deg/sec reported during *Fishhook Maneuver* vehicle rollover testing specified by NHTSA [22-24]. Figure 6 shows the time histories of left wheel displacement (thin-solid line), right wheel displacement (dot line) and vehicle roll angular displacement (thick-solid line) when the impulsive moment is applied at t=0.1 sec for the duration of only 0.01 sec. Results show a heavily damped roll response and wheel and roll displacements damp out in about 1.5 sec. The maximum roll displacement is about 0.090 rad (~5.2 deg), occurring at t=0.185 sec.

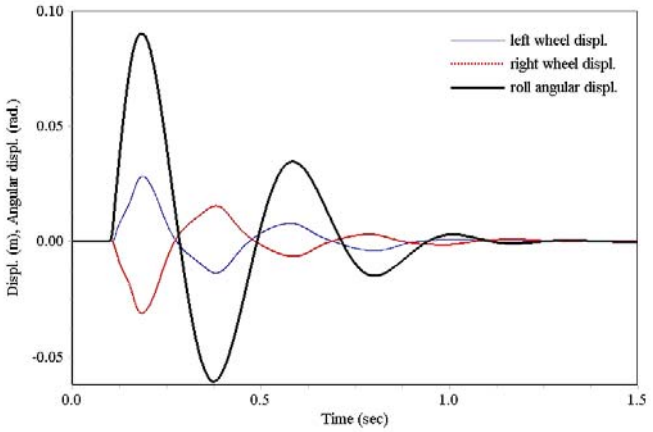

Figure 6: Wheel and roll displacements of the half-car model due to impulse roll moment of 50 kNm.

As described in Section 2, the characteristics of cylinder and accumulator valves are highly nonlinear and therefore the dynamic properties such as roll stiffness and damping coefficients are highly depend on the magnitude of the roll displacement. In addition, the damper valves have asymmetric damping properties and provide flow resistance in only one direction. When the roll angle is very small, the force due to the pressure differential across the spool valves is not large enough to overcome the spring preload to open the damper valves and therefore the roll dynamics are governed by fluid flow through bleed holes of the valves. When the roll angle is high, the dynamic response is dominated by rapid opening and closing of damper valves accompanied by large fluid motions, i.e., the operating region is in the second ramp of the damper valve characteristics shown in Figure 4.

The spool displacement profiles of the valves show when a large impulsive roll moment of 50 kNm is applied, the cylinder and accumulator valves are opened for open for about 1.0 sec. The best measure of effective roll stiffness is calculated from the roll response after t=1.0 sec. The analysis of time history of roll displacement shows that the effective roll stiffness and roll damping are about 240 kNm/rad and 30%, respectively. This dynamic roll stiffness is significantly higher that the static roll stiffness of 124 kNm/rad. Results presented in Figure 6 also show the maximum wheel displacement of 29 mm occurring at t=0.18 sec.

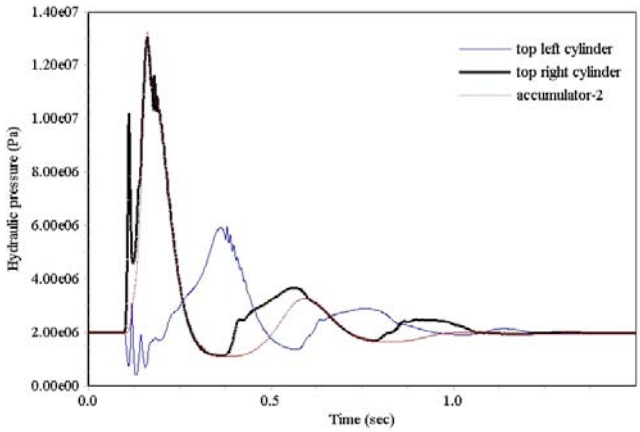

Figure 7: Typical pressure traces of the half-car model due to impulse roll moment of 50 kNm.

Figure 7 shows typical hydraulic pressure profiles of the half-car model when an impulsive roll moment of 50 kNm is applied. Only pressure profiles corresponding to top-left cylinder (thin-solid line), top-right cylinder (thick-solid line) and accumulator-2 (dot line) are presented. The impulsive moment simulates an initial role rate of 105 deg/sec and therefore the initial pressure at top-right cylinder is significantly higher than the mean operating pressure. In particular, the maximum top-right cylinder pressure is about 13.0 MPa, occurring at t=0.16 sec. The maximum top-left cylinder pressure is about 6.0 MPa, occurring at t=0.36 sec. As shown in Figure 3, the accumulator-2 is located in the hydraulic line-2 and linked to the top-right cylinder and therefore accumulator pressure-2 closely resembles that of the top-right cylinder pressure. The initial pressure increase in the top-right cylinder is accompanied by significant flow to the accumulator-2 of the HIS system. The cylinder and accumulator pressures continue to oscillate about the mean pressure of 2.0 MPa until about t=1.5 sec.

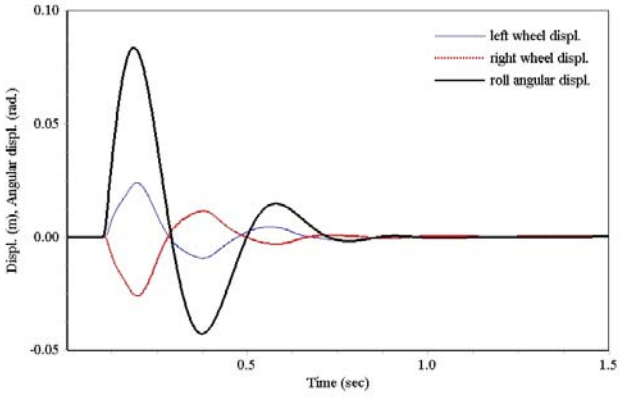

Figure 8: Wheel and roll displacements of the full-car model due to impulse roll moment of 100 kNm.

Simulation is also performed with the full-car configuration and the corresponding results for an impulsive roll moment of 100 kNm are shown in Figures 8 and 9. Figure 8 shows the time histories of left wheel displacement (thin-solid line), right wheel displacement (dot line) and vehicle roll angular displacement (thick-solid line) when the impulsive moment is applied at t=0.1 sec for the duration of 0.01 sec. For clarity, only the front wheel displacements of the full-car model are presented in Figure 8. However, the comparison of the front- and back-wheel displacements (results not presented here) indicates very similar effective stiffness and damping characteristics. It is noted that the accumulators of the HIS system are located near the front wheels of the vehicle and therefore the stiffness of the back wheels is slightly higher than that of the front wheels.

The analysis of roll displacement shows that the effective roll stiffness and roll damping are about 308 kNm/rad and 49%, respectively. Results also show that the maximum roll displacement is about 0.083 rad (~4.8^{o}), occurring at t=0.185 sec. The pressure profiles of top-left cylinder (thin-solid line), top-right cylinder (thick-solid line) and accumulator-2 (dot line) are shown in Figure 9. The maximum top-right and top-left cylinder pressures are 10.9 MPa and 4.6 MPa, respectively.

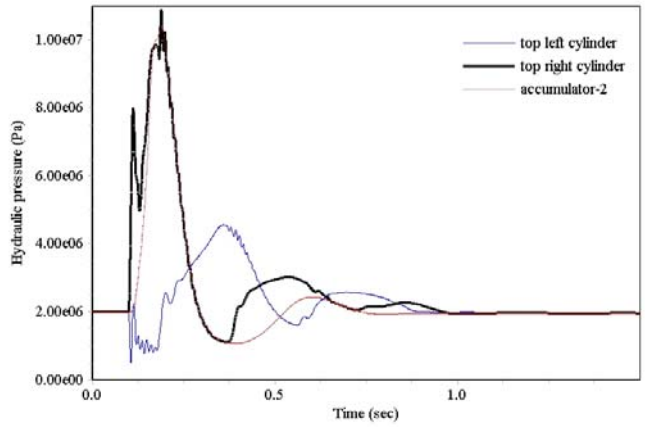

Figure 9: Typical pressure traces of the full-car model due to impulse roll moment of 100 kNm.

The direct comparison of roll displacement of the half- and full-car models is presented in Figure 10. Results show the time histories of roll displacement are similar but the half-car model overestimates the vehicle roll displacement. In particular, the initial maximum roll displacement predicted by the half-car model is 0.090 rad. This is about 8% higher than the corresponding value of 0.083 rad predicted by the full-car model. The wheel and roll displacements of the full-car model exhibit faster decay rates and the half-car model underestimates roll stiffness and roll damping coefficients. In particular, the roll stiffness and roll damping predicted by the half-car model are 24% and 38% lower than the corresponding values predicted by the full-car model, respectively. This is also evident from the cylinder pressure profiles of the half- and full-car models compared in Figure 11. The maximum top-right cylinder pressure predicted by the half-car model is about 13.0 MPa compared to 10.9 MPa predicted by the full-car model. The right cylinder pressure oscillations predicted by the full-car model damp out very quickly. In general, consistent trends are noted when comparing the roll response of the half- and full-car models of the HIS system, i.e., the half-car model underestimates the effective stiffness and damping ratio during large amplitude roll motion.

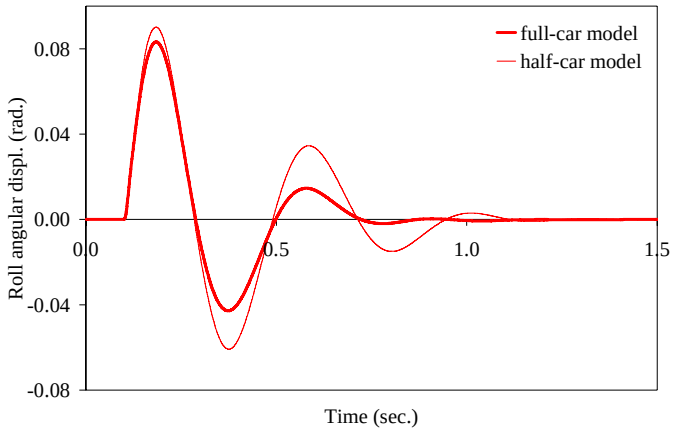

Figure 10: Comparison of roll displacements of full-and half-car models due to impulse roll moment.

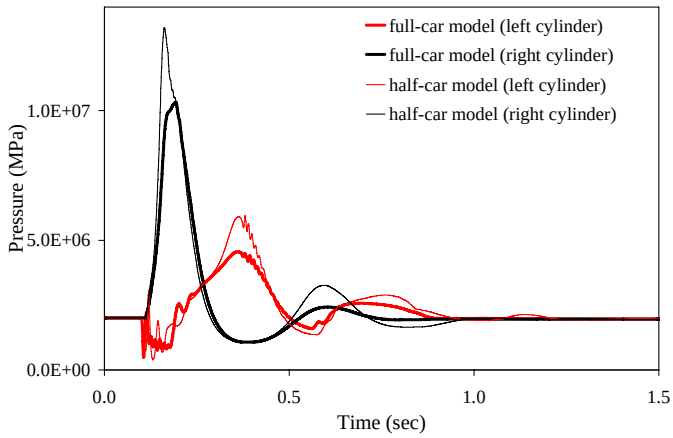

Figure 11: Comparison of pressure profiles of full-and half-car models due to impulse roll moment.

To investigate the vehicle bounce response of the HIS system, the simulation is performed for an impulsive force of 100 kN applied at the centre of gravity of the sprung mass for a duration of 0.01 sec. Because of the assumed left-right symmetry, the time history of all four wheel displacements are of the same magnitude and the roll and pitch displacements are zero. Figure 12 shows the time history of wheel displacement (dot line) and vehicle bounce displacement (thick-solid line). The displacement profiles show a highly damped bounce response with an equivalent damping ratio of about 54%. The maximum bounce is about 79.2 mm, occurring at t=0.30 sec. Analysis shows that the effective stiffness of the bounce motion is 73.5 kN/m.

Given that the actual stiffness of the four suspension springs is 80 kN/m (see Table 1, stiffness of each suspension spring is 20 kN/m), the HIS system of the full-car model softens the bounce motion by about 8%.

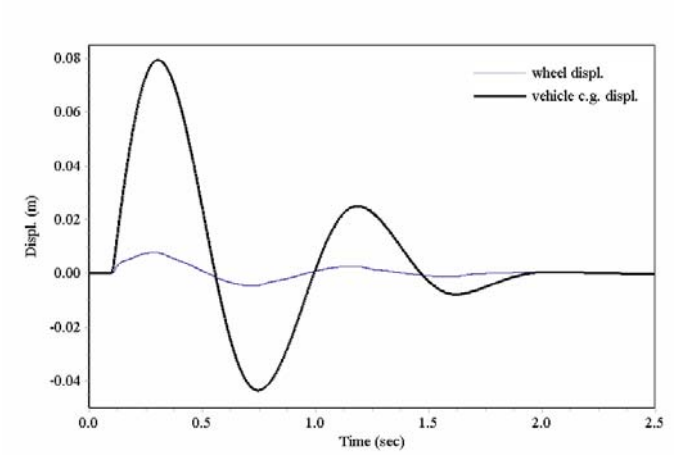

Figure 12: Wheel and bounce displacements of the full-car model due to impulse bounce of 100 kN.

To illustrate the effects of hydraulic pressures on vehicle bounce response, typical pressures of bottom cylinder (thin-solid line), top cylinder (thick-solid line) and accumulator-1 (dot line) are shown in Figure 13. Due to the initial impulse bounce rate of about 700 mm/sec, the initial pressure in the bottom cylinders overshoots to about 5.0 MPa immediately after the impulsive force is applied at t=0.1 sec. With the absence of the roll motion, the pressure oscillations in the cylinders and accumulators are significantly lower than the values presented for the vehicle roll motion (see Figure 9). In particular, the maximum accumulator pressure registered is only about 2.3 MPa.

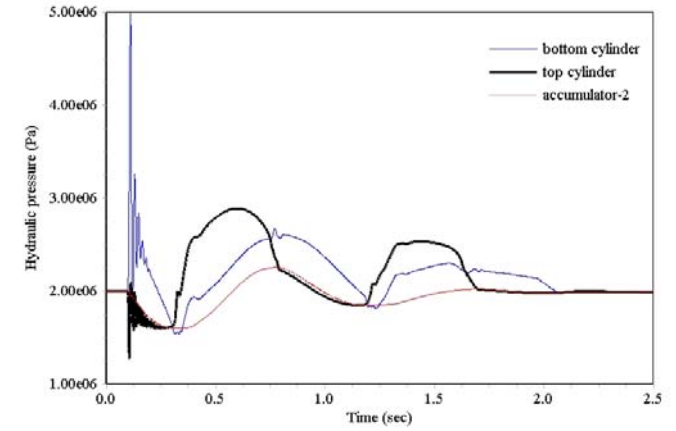

Figure 13: Typical cylinder and accumulator pressures of the full-car model due to impulse bounce force of 100 kN.

The direct comparison of bounce displacement of the half- and full-car models is presented in Figure 14. The time history of bounce and wheel displacements are almost indistinguishable and the analysis shows that the effective stiffness and damping coefficient of the vehicle bounce from the half- and full-car models are within 1%. The simplified half-car model therefore captures the essential dynamics of the bounce motion.

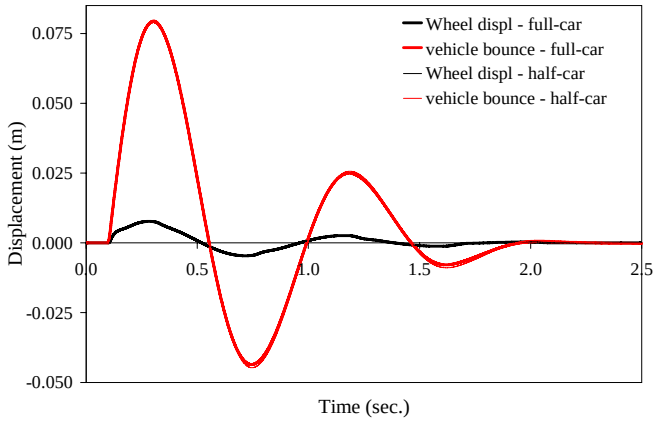

Figure 14: Comparison of wheel and vehicle bounce displacements of full- and half-car models due to impulse bounce force.

The vehicle pitch motion of the HIS system is evaluated by applying an impulsive pitch moment of 100 kNm at the centre of gravity of the sprung mass for a duration of 0.01 sec. Because of the assumed left-right symmetry of the HIS system, the time history of roll displacement is zero. Figure 15 shows the back-wheel displacement (dot line), front wheel displacement (thick-solid line) and vehicle pitch angular displacement (thin-solid line). Results also show that the maximum pitch displacement is about 0.042 rad (~2.4^{o}), occurring at t=0.26 sec. The analysis of pitch displacement shows that the initial effective pitch stiffness and pitch damping are about 160 kNm/rad and 60%, respectively.

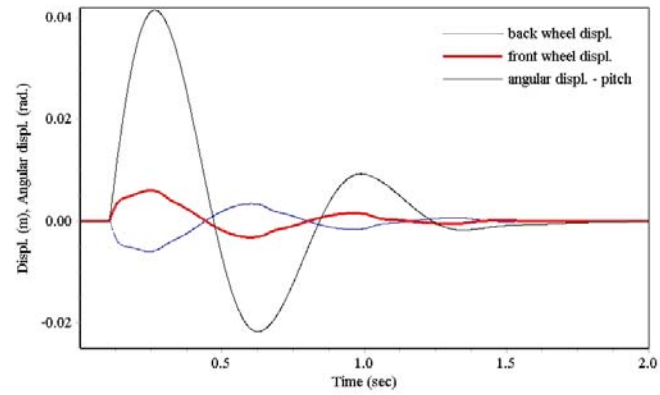

Figure 15: Wheel displacements and pitch angular displacements of the full-car model due to impulse pitch moment of 100 kNm.

To illustrate the effects of hydraulic pressures on vehicle pitch motion, typical pressure traces of bottom cylinder (thin-solid line), top cylinder (thick-solid line) and accumulator-1 (dot line) are shown in Figure 16. For

clarity, only the front cylinder pressures are presented. The initial pressure oscillations in the top and bottom cylinders are due to the large impulse pitch motion applied at t=0.1sec. In general, the pressure oscillations in the cylinders are significantly lower than the values presented for the vehicle roll motion (see Figure 9). In the absence of roll motion, there is no flow to the accumulators and the accumulator pressure remains constant at the mean pressure of 2.0 MPa.

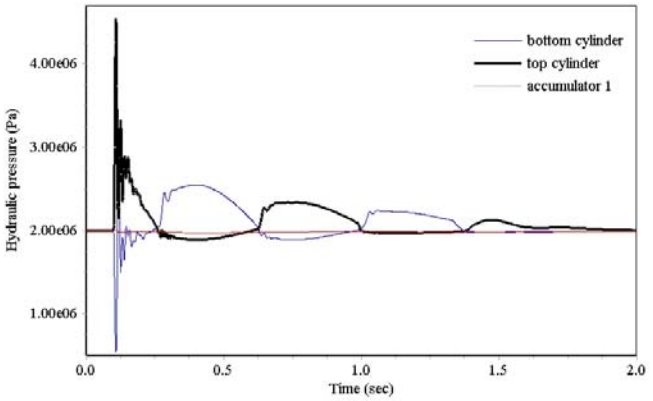

Figure 16: Typical cylinder and accumulator pressures of the full-car model due impulse pitch moment of 100 kNm.

CONCLUSION

A vehicle dynamic model that captures the transient characteristics of a HIS system is presented. The vehicle is modelled as a lumped mass system with a half-car model with four-degrees-of-freedom and a full-car model with seven-degrees-of-freedom. The lumped mass full-car model includes the roll, bounce and pitch motions of the vehicle and vertical movements of the four wheel-stations. Mathematical models are developed to represent the nonlinearities associated with pressure-flow characteristics, fluid properties, damper valves, accumulators and coupling between mechanical and fluid systems. The transient performance is demonstrated by numerical integration of the second-order nonlinear differential equations, utilizing the Runge-Kutta fourth order integration scheme.

The HIS system performance is evaluated from the time history of displacements when the sprung mass is subjected to impulsive forces and moments. Simulation results show that a simplified half-car model captures the essential dynamics of the vehicle bounce motion, however, it overestimates the displacements and hydraulic pressures during vehicle roll motion. The half-car model underestimates the effective stiffness and damping ratio of the HIS system during large amplitude roll motion and the coupling effects of the HIS system are best represented by the full-car model. The HIS system provides improved roll stability by significantly enhancing roll stiffness without altering bounce stiffness and damping properties. The developed nonlinear models provide insight into various hydraulic system parameters and nonlinearities, and reveal directions for design improvements for vehicles fitted with similar HIS systems.

ACKNOWLEDGMENTS

Financial support for this research is provided jointly by the Australian Research Council (ARC LP0562440) and University of Technology, Sydney.

REFERENCES

1. F.C. Mock, Relation of spring-suspension to riding qualities, *SAE Paper 260045*, 1926.
2. O.D. Dillman, E.J. Collier, Building stability into the modern automobile, *SAE Paper 530036*, 1953.
3. T.D. Gillespie, TD, Fundamentals of Vehicle Dynamics, *SAE International*, Warrendale, Pa., 1992.
4. F.N. Beauvais, C. Garelis, D.H. Iacovoni, An improved analog for vehicle stability analysis, *SAE Paper 610161*, 1961.
5. A.E. Moulton, A Best, Hydragas suspension, *SAE Paper, 790374*, 1979.
6. R.S. Sharp, D.A. Crolla, Road vehicle suspension system design - a review, *Vehicle System Dynamics,* 16 (1987) 167-192.
7. W. Bolton, Pneumatic and hydraulic systems, Butterworth-Heinemann, Oxford, 1997.
8. E. Zapletal, Balanced suspension, Proc. of the 2000 SAE Motorsports Engineering Conference & Exposition, 2000.
9. M.C. Smith, and F.C. Wang, Performance benefits in passive vehicle suspensions employing inerters, *Proc. of the 42nd IEEE Conf. on Decision and Control*, 2003, pp. 2258-2263.
10. M. Milanese, C. Novara, P. Gabrielli, L. Tenneriello, Experimental modelling of vertical dynamics of vehicles with controlled suspensions, *SAE Paper 2004-01-1546*, 2004.
11. R. Cooke, D.A. Crolla, M. Abe, Modelling combined ride and handling maneuvers for a vehicle with slow-active suspension, *Vehicle System Dynamics*, 27 (5-6) (1997) 457-476.
12. N.D. Sims, R. Stanway, Semi-active vehicle suspension using smart fluid dampers: a modelling and control study, *International Journal of Vehicle Design*, 33 (1-3) (2003) 76-102.
13. J. Watton, K.M. Holford, P. Surawattanawan, Electrohyraulic effects on the modelling of a vehicle active suspension, *Proc. IMechE., Part D: Journal of Automobile Engineering, 215* (6) (1991) 1077-1092.
14. M. Ortiz, Principles of interconnected suspension, *Racecar Engineering*, 7 (1997) 7-8.
15. N. Mace, Analysis and synthesis of passive interconnected vehicle suspensions, PhD Thesis, University of Cambridge, 2004.
16. S. Rakheja, P.J. Liu, A.K.W. Ahmed, H. Su, Analysis of an interlinked hydro-pneumatic

suspension, *Advanced Automotive technologies*, 52 (1993) 279-287.
17. P.J. Liu, S. Rakheja, A.K.W. Ahmed, Properties of an interconnected hydro-pneumatic suspension system, *Transactions of the Canadian Society for Mechanical Engineering,* 19 (4) (1995) 383-396.
18. P.J. Liu, S. Rakheja, A.K.W. Ahmed, An analytical study of an interconnected vehicle suspension, *Advanced Automotive Technologies,* 56 (1995) 151-160.
19. C.B. Heyring, Vehicle suspension system, *United States Patent 5480188*, 1996.
20. J. Fontdecaba, Integral suspension system for motor vehicles based on passive components, *SAE Paper 2002-01-3105*, 2002.
21. M.C. Smith, G.W. Walker, Interconnected vehicle suspensions, *Proc. IMechE., Part D: Journal of Automobile Engineering*, 219 (2005) 295-307.
22. J.R. Wilde, G.J. Heydinger, D.A. Guenther, T. Mallin, A.M. Devenish, Experimental evaluation of fishhook maneuver performance of a Kinetic™ suspension system, *SAE Paper 2005-01-0392*, 2005.
23. W.R. Garrott, G.J. Forkenbrock, J.G. Howe, Results from NHTSA's experimental examination of selected maneuvers that may induce on-road untripped, light vehicle rollover, *SAE Paper 2001-01-0131*, 2001.
24. G.J. Forkenbrock, W.R. Garrott, M. Heitz, B.C. O'Harra, An experimental examination of J-turn and fishhook maneuvers that may induce on-road, untripped, light vehicle rollover, *SAE Paper 2003-01-1008*, 2003.
25. N. Zhang, W. Smith, J. Jeyakumaran, Free vibration of vehicles with hydraulically interconnected suspensions, *Journal of Sound and Vibration*, Submitted for publication, 2006.
26. D. McCloy, H.R. Martin, Control of Fluid Power: Analysis and Design, 2nd (revised) Edition, Chichester, England, 1980, pp. 236-240.
27. Y. Liu, J. Zhang, F. Yu, H. Li, Test and simulation of nonlinear dynamics response for the twin-tube hydraulic shock absorber, *SAE Paper 2002-01-0320*, 2002.
28. S.A. Mughal, Coefficient of discharge and mass flow rate for reed type valves, *Proc. Multi-phase Flow and Heat Transfer Symposium*, 2 (1979) 1191-1204.
29. K.A. Edge, D.N. Johnston, The impedance characteristics of fluid power components: relief valves and accumulators, *Proc IMechE, Part I: Journal of Systems and Control Engineering*, 205 (1991) 11-22.

CONTACT

Jeku M. Jeyakumaran

Mechatronics and Intelligent Systems
Faculty Of Engineering
University of Technology, Sydney
PO Box 123, Broadway
NSW, Australia

Ph: (02) 9514 1613
Fax: (02) 9514 2655
email: jeku.jeyakumaran@uts.edu.au

NOMENCLATURE

A_i	Cross sectional area of pipe element *i*
A_0	Effective flow area of the orifice
b_j	Lateral distance from the vehicle body c.g. to suspension strut
c_d	Fluid discharge coefficient
c_{tj}	Damping coefficient of tire
c_{sj}	Damping coefficient of piston strut
F_p	Pressure force on the piston/spool
F_s	Spring force on the piston/spool
F_d	Damping force on the piston/spool
F_f	Flow force on the piston/spool
F_{kj}	Force between vehicle body and road wheel due suspension spring
F_{hj}	Force between vehicle body and road wheel due to HIS system
I_θ	Sprung mass moment of inertia about roll plane
k_i	Viscous loss factor pipe element *i*
k_{sj}	Stiffness of suspension springs
k_{tj}	Stiffness of the tire
l_i	Length of the pipe element *i*
M	Sprung mass of the vehicle body
m_j	Unsprung mass of the wheel-station
m_s	Mass of piston/spool
p	Pressure
$\dot{p}$	Time derivative of pressure
p_0	Precharge gas pressure in accumulator
Q	Flow rate
$\dot{Q}_i$	Time derivative of the flow rate
Q_i	Mean flow through pipe element *i*
$Q_{i,in}$	Input flow to the pipe junction *i*
$Q_{i,out}$	Output flow from the pipe junction *i*
V	Fluid volume
V_0	Precharge gas volume in accumulator
x_s , $\ddot{x}_s$	Displacement/acceleration of the piston/spool
$y_{Gj}, \dot{y}_{Gj}$	Vertical displacement/velocity of tire-

	ground contact patch
$y_v, \dot{y}_v, \ddot{y}_v$	Vertical displacement / velocity / acceleration of vehicle body c.g.
$y_{vj}, \dot{y}_{vj}, \ddot{y}_{vj}$	Vertical displacement / velocity / acceleration of one side of vehicle body
$y_{wj}, \dot{y}_{wj}, \ddot{y}_{wj}$	Vertical displacement / velocity / acceleration of road wheel-station
Greek letter	
ρ	Density of the oil
μ	Viscosity of the oil
β	Bulk modulus of the oil
γ	Ratio of specific heat for nitrogen
$\theta, \dot{\theta}, \ddot{\theta}$	Angular displacement / velocity / acceleration of vehicle body-roll plane
Subscripts	
i	Pipe element *i* with constant diameter
j	Left or right side, i.e., l or r
1	upstream of a flow restrictor
2	downstream of a flow restrictor
i1, i2	End 1 and 2 of the pipe element *i*